

Lasing properties of an Yb ion in tetragonal $LuPO_4$ and $LuVO_4$ isomorphic crystals:a comparative study

Xiao-Dan Dou(窦晓丹), Jing-Nan Yang(杨婧男), Jie He(贺杰), Li-Sha Wang(王丽莎), Wen-Juan Han(韩文娟), Hong-Hao Xu(徐洪浩), De-Gao Zhong(钟德高), Bing Teng(滕冰), Jun-Hai Liu(刘均海)
Citation: Chin. Phys. B . 2018, 27(5): 054211. **doi:** 10.1088/1674-1056/27/5/054210

Journal homepage: http://cpb.iphy.ac.cn; http://iopscience.iop.org/cpb

What follows is a list of articles you may be interested in

Tunable second harmonic generation from a Kerr-lens mode-locked Yb: $YCa_4O(BO_3)_3$ femtosecond laser

Zi-Ye Gao(高子叶), Jiang-Feng Zhu(朱江峰), Zheng-Mao Wu(吴正茂), Zhi-Yi Wei(魏志义), Hao-Hai Yu(于浩海), Huai-Jin Zhang(张怀金), Ji-Yang Wang(王继扬)
Chin. Phys. B . 2017, 26(4): 044202. **doi:** 10.1088/1674-1056/26/4/044202

A single-longitudinal-mode continuous-wave Ho^{3+}: YVO_4 laser at 2.05 μm pumped by a Tm-fibre laser

Jing Wu(吴婧), Youlun Ju(鞠有伦), Zhenguo Zhang(张振国), Liwei Xu(徐丽伟), Tongyu Dai(戴通宇), Baoquan Yao(姚宝权), Yuezhu Wang(王月珠)
Chin. Phys. B . 2017, 26(1): 014204. **doi:** 10.1088/1674-1056/26/1/014204

Diode-pumped Kerr-lens mode-locked femtosecond Yb:YAG ceramic laser

Zi-Ye Gao(高子叶), Jiang-Feng Zhu(朱江峰), Ke Wang(汪珂), Jun-Li Wang(王军利), Zhao-Hua Wang(王兆华), Zhi-Yi Wei(魏志义)
Chin. Phys. B . 2016, 25(2): 024205. **doi:** 10.1088/1674-1056/25/2/024205

Diode-pumped self-starting mode-locked femtosecond Yb：$YCa_4O(BO_3)_3$ laser

Gao Zi-Ye, Zhu Jiang-Feng, Tian Wen-Long, Wang Jun-Li, Wang Qing, Zhang Zhi-Guo, Wei Zhi-Yi, Yu Hao-Hai, Zhang Huai-Jin, Wang Ji-Yang
Chin. Phys. B . 2014, 23(5): 054207. **doi:** 10.1088/1674-1056/23/5/054207

A narrow-linewidth continuous wave Ho：$YALO_3$ laser with Fabry–Perot etalons

Yang Xiao-Tao
Chin. Phys. B . 2014, 23(3): 034207. **doi:** 10.1088/1674-1056/23/3/034207

High-power ultraviolet 278-nm laser from fourth-harmonic generation of an Nd:YAG amplifier in CsB_3O_5 crystal*

Miao He(何苗)[1,2,3], Feng Yang(杨峰)[1,2,†], Cheng Dong(董程)[1,2,3], Zhi-Chao Wang(王志超)[1,2], Lei Yuan(袁磊)[1,2], Yi-Ting Xu(徐一汀)[1,‡], Guo-Chun Zhang(张国春)[2], Zhi-Min Wang(王志敏)[1,2], Yong Bo(薄勇)[1,2], Qin-Jun Peng(彭钦军)[1,2], Da-Fu Cui(崔大复)[1], Yi-Cheng Wu(吴以成)[2], and Zu-Yan Xu(许祖彦)[1,2]

[1] *Key Laboratory of Solidstate Laser, Technical Institute of Physics and Chemistry (TIPC), Chinese Academy of Sciences, Beijing* 100190, *China*
[2] *Key Laboratory of Functional Crystal and Laser Technology, TIPC, Chinese Academy of Sciences, Beijing* 100190, *China*
[3] *University of Chinese Academy of Sciences, Beijing* 100049, *China*

(Received 17 December 2017; revised manuscript received 5 January 2018; published online 26 April 2018)

We report on the experimental investigation and theoretical analysis of a nanosecond pulse high power ultraviolet (UV) 278 nm laser by fourth-harmonic generation (FHG) of a 1112-nm Nd:YAG amplifier in LiB_3O_5 (LBO) and CsB_3O_5 (CBO) crystals. The UV laser delivers a maximum average power of 10.3 W at 278 nm with peak power of 36.8 kW under input pump power of 41 W at 556 nm. This is, to the best of our knowledge, the highest output power at the specific UV wavelength of 278 nm. We also performed the theoretical investigation on the FHG with a model in the Gaussian approximation of both spatial and temporal profiles, especially accounting for the two-photon absorption effect in CBO crystal for the first time. The average output power, pulse width, and beam spatial distribution of the UV laser were simulated. The theoretical calculations are in close agreement with the experimental results.

Keywords: ultraviolet lasers, frequency doubled, CsB_3O_5 (CBO) crystal, two-photon absorption

PACS: 42.55.Xi, 42.65.Ky, 42.72.Bj **DOI:** 10.1088/1674-1056/27/5/054211

1. Introduction

High power all-solid-state ultraviolet (UV) lasers have been in demand for various industrial and scientific applications, such as laser marking, drilling, cutting on printed circuit boards (PCBs), rapid prototyping and spectroscopy due to its low maintenance cost, small system size, long lifetime and high efficiency compared with other UV lasers.[1–3] Especially, UV lasers with a wavelength between 275 and 300 nm exhibit the characteristics of special waveband located in the solar-blind UV region with high photon energy. Also, they are always the most attractive laser source for atmospheric remote sensing, communications and molecule detection.

So far, the most effective approach to achieving UV lasing between 275 and 300 nm is based on fourth-harmonic generation (FHG) from a near-infrared solid state fundamental laser with a wavelength between 1100 nm and 1200 nm by means of nonlinear optical (NLO) crystals. This has resulted in the rapid development of high-quality NLO crystals such as β-$Ba_2B_2O_4$ (BBO),[4] LiB_3O_5 (LBO),[5] CsB_3O_5 (CBO),[6,7] $CsLiB_6O_{10}$(CLBO),[8] $K_3B_6O_{10}Cl$ (KBOC),[9] etc. Based on these UV NLO crystals, significant progress has been made in this field over the past decade. Unfortunately, the highest output powers reported were less than one watt.[10–12] In order to increase detection range and accuracy, more output power or pulse energy is demanded. Recently, a significant improvement in laser output was demonstrated with CBO as UV NLO crystal. For instance, up to 1.5 W UV lasing at 278 nm was produced from a frequency quadrupled 1112 nm Nd:YAG laser in CBO crystal for the first time.[13] By adopting a similar construction, a 1.3 W UV laser at 281 nm was produced from FHG of a 1123-nm Nd:YAG laser.[14] The results indicate that the CBO crystal is suitable for efficient UV generation for wavelengths between 275 and 300 nm. However, further power scaling of the UV laser is limited, mainly by the available output power of the high beam quality 1.1 μm fundamental pump sources owing to their smaller stimulated cross-section areas and larger quantum defect compared to the 1064 nm line.[15] An effective scheme to solve this problem is to use master oscillator power amplifier (MOPA) technology.[16,17] Moreover, shortening the pulse width to achieve higher peak power and adopting an appropriate long NLO crystal are also beneficial to enhance the cascaded frequency conversion efficiency, all contributing to achieving a high UV output power.

We present a record-high average power all-solid-state UV laser at 278 nm by the FHG of a 1112-nm Nd:YAG MOPA

*Project supported by the National Natural Science Foundation Program of China (Grant Nos. 11504389 and 61505226), the National Key Research Development Program of China (Grant Nos. 2016YFB040203 and 61535013), and the National Development Project for Major Scientific Research Facility of China (Grant No. ZDYZ2012-2).

†Corresponding author. E-mail: yang12345yang@163.com
‡Corresponding author. E-mail: xuyiting1984@sina.com.cn

© 2018 Chinese Physical Society and IOP Publishing Ltd

laser for the first time. A homemade 75.5 W nanosecond (ns) pulsed 1112 nm MOPA Nd:YAG laser was adopted as the infrared (IR) fundamental source. The frequency quadrupling was performed by two-stage SHG in LBO and CBO crystals, subsequently. With a 30 mm-long CBO crystal, we successfully scaled the UV average output power up to 10.3 W, which is almost seven times higher than the previous best result in Ref. [13]. The UV laser operated at a pulse repetition rate (PRR) of 2 kHz with the pulse duration of 140 ns, corresponding to a peak power of 36.8 kW. To the best of our knowledge, this is the highest output in terms of both average power and peak power for an all solid-state UV laser between 275 and 300 nm. In comparison with the experiment, we employ a numerical model accounting for two-photon absorption (TPA) effect of the UV beam in crystal for the first time to describe the ns type-I SHG of CBO and to analyze the influence of TPA on UV generation. The dependence of the UV average output power on the pump power at 556 nm was calculated and the effect of the TPA was discussed. The spatial and temporal characteristics of the pulsed 278 nm beam were also simulated.

2. Experimental setup

The experimental setup of the high power all-solid-state UV laser system is illustrated in Fig. 1. Compared to our previous work,[13] here, we developed a 1112-nm NdYAG MOPA system in order to achieve a higher-power fundamental pump laser while maintaining high beam quality. The Nd:YAG MOPA system consisted of a 1112 nm Nd:YAG oscillator, and first-stage double pass and two-stage single pass diode-side-pumped Nd:YAG amplifiers. The oscillator delivered a maximum output power of 25.2 W with beam quality factor M^2 of 1.46 at a PRR of 2 kHz with the pulse duration of 210 ns. In Fig. 1, AH1–AH6 are identical diode-side-pumped Nd:YAG amplifier heads. Each Nd:YAG rod (Φ3 mm×72 mm) was doped with 0.6 at.% concentration of Nd^{3+} and antireflection (AR) coating at 1064 and 1112 nm on both end faces. There were three quasi-continuous wave (QCW) laser diode (LD) arrays arranged in a three-fold symmetry around the laser crystal rod and each diode array with four 20 W diodes operating at 808 nm with pump pulse duration of 160 μs and PRR of 1 kHz, respectively. A 90° quarter rotator (QR) was inserted between the amplifier heads for compensating the thermal-induced birefringence. f1–f6 are the convergent lenses with AR coating at 1112 nm for mode matching. TFP1 is a thin film polarizer with reflection (HR) coating at 1112 nm in the perpendicular (s-polarized) direction and high transmission (HT) coating in the parallel (p-polarized) direction with an incident angle of 45°. QWP is a quarter-wave plate at 1112 nm. M1–M4 are flat mirrors coated with HR at 1112 nm and AR at 1064 nm. Once the p-polarized seed laser was injected into the amplifier chain through TFP1, it was amplified by AH1 and AH2 firstly. By means of QWP, the beam after a round trip would change its polarization state to the orthogonal direction. Therefore, the forward beam was reflected by mirror M1 and re-imaged into the gain medium to get the second-pass amplification. Afterwards, the amplified beam returned from the double-pass stage, was reflected by TFP1 and entered the following two-stage single pass amplifiers through AH3–AH4 and AH5–AH6.

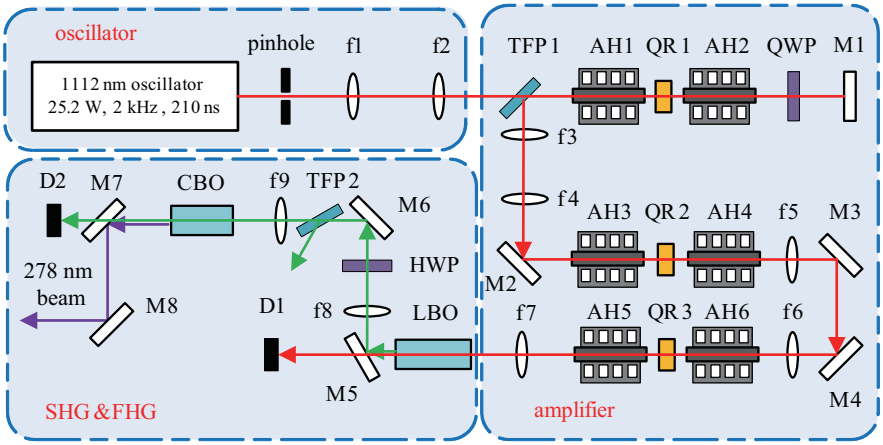


Fig. 1. (color online) Experimental setup of the UV 278 nm laser. F1–F9: convergent lenses; TFP1, TFP2: thin film polarizers; AH1–AH6: diode-side-pumped Nd:YAG amplifier heads; QR1–QR3: 90° quarter rotators; QWP: quarter-wave plate; M1–M8: flat mirrors; HWP: half-wave plate; D1–D2: dump.

The amplified fundamental beam was collimated through lens F7 into the type-I noncritical phase-matched LBO crystal cut at $\theta = 90°$ and $\varphi = 0°$ with a dimension of $4 \times 4 \times 40$ mm^3. The temperature of the LBO was kept at 95.1 °C by a proportional integral differential (PID) temperature controller with the controlling precision of ±0.1 °C. Both the entrance and the exit surfaces of the LBO crystal were AR-coated at 1112 nm and 556 nm. The generated 556-nm green beam and the residual IR beam were separated by two dichroic mirrors, M5 and M6, which were AR-coated at 1112 nm and HR-coated at

556 nm. The residual 1112 nm fundamental source was collected by dump D1. The green laser beam was then collimated by lens F8 and focused by lens F9 into a high-quality type-I CBO crystal cut at $\theta = 74.9°$ and $\varphi = 90°$. In order to enhance the nonlinear conversion efficiency leading to higher UV power, a 30-mm-long CBO crystal was employed instead of previous 13-mm-long crystal.[13] The half-wave plate (HWP) and TFP2 were utilized as a power attenuator to adjust the injected green pump power. The CBO crystal was wrapped in aluminum foil and placed in a copper heat sink for cooling. Both the entrance and the exit surfaces were optically polished and uncoated. The linear absorption coefficient of the CBO crystal is about 0.05 cm^{-1} at 556 nm and 0.07 cm^{-1} at 278 nm, respectively. Two dichroic mirrors, M7 and M8, with HR at 278 nm and AR at 556 nm were used to separate the residual green beam from the generated UV beam. The UV output power was measured by a power meter (OPHIR Photonics FL30A-BB-18 ROHS) and the residual green beam was collected by another dump. D2.

3. Experimental results and theoretical analysis

In the experiment, a 25.2 W seed laser at 1112 nm was amplified by the three-stage Nd:YAG amplifiers and the output power was scaled up to 75.5 W with beam quality M^2 of 2.79. Once frequency was doubled by the LBO crystal, a maximum output power of 51.9 W at 556 nm was obtained, corresponding to an SHG conversion efficiency of 68.7%. Such a high conversion efficiency is, to the best of our knowledge, the highest for SHG in this wavelength region. The beam quality of the green laser was measured as $M_x^2 = 1.9$ and $M_y^2 = 2.1$ in the orthogonal directions, respectively. Next, the second0stage SHG was carried out in CBO crystal. The UV average output power at 278 nm as a function of the injected green pump power at 556 nm was measured as shown in Fig. 2 by red filled circles. It can be seen from Fig. 2 that the UV output power grows monotonically with the increasing input power and shows no signs of saturation. A highest average output power of 10.3 W was obtained under an incident green pump power of 41 W, corresponding to an SHG conversion efficiency of 25.1% from green to UV, which is more than two times higher than the previous demonstration reported in Ref. [13]

The spectrum of the generated UV laser was monitored by an optical spectrum analyzer (AvaSpec-2048FT-SPU) at the maximum output power as exhibited in Fig. 3, which indicates that the UV wavelength was centered at 277.74 nm with a linewidth of $\Delta\lambda = 0.68$ nm. The pulse temporal profile was recorded by an oscilloscope (Tektronix, DPO4104B-L) with a fast photodiode detector (THORLABS, DET10N/M). A typical oscilloscope trace of the pulse is presented with a pulse width of about 140 ns at the maximum output power as the blue curve shown in Fig. 4. In accord with the fundamental laser source, the PRR of the UV laser is 2 kHz as well. The corresponding pulse energy and peak power were 5.2 mJ and 36.8 kW, respectively. This high peak power is roughly higher two orders of magnitude higher than the previous results reported in Refs. [13] and [14] (500 W and 620 W, respectively).

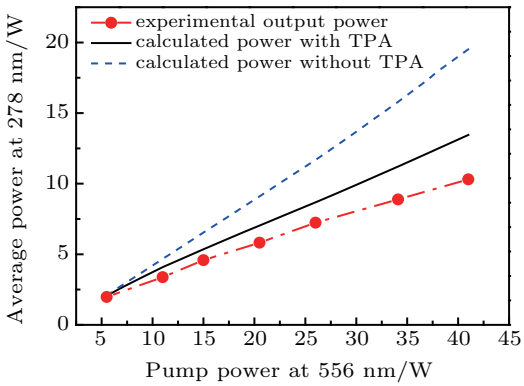


Fig. 2. Average output power at 278 nm laser as a function of the pump power at 556 nm.

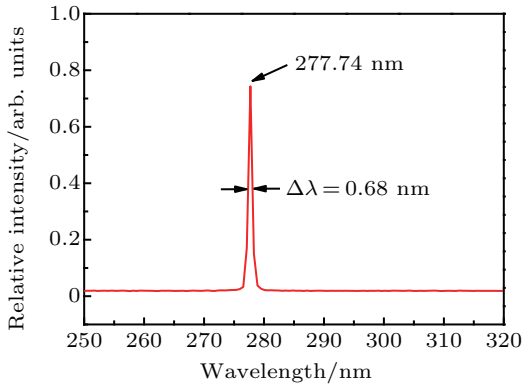


Fig. 3. Measured spectrum of the UV laser.

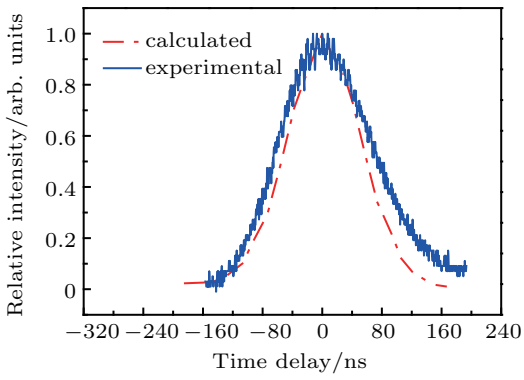


Fig. 4. Measured and calculated pulse profile of the UV 278 nm laser.

In order to get a deep insight into the UV output characterization, a set of coupled-wave equations were used to describe the SHG from green to UV in CBO. In our numerical model, the Gaussian approximation of both spatial and temporal profiles was employed, considering spatial birefringence walk-off, pump depletion and linear absorption loss of each wave. Especially, the TPA effect was taken into account. Then the propagation of ns pulse envelope A_i along the longitudinal coordinate z during the SHG for type-I (ee→o) can be expressed as follows:[18–20]

$$\frac{\partial A_1}{\partial z} = \mathrm{j}\sigma_1 A_2 A_1^* \exp(\mathrm{i}\Delta k z) - \frac{\alpha_1}{2}A_1 - \tan\rho\frac{\partial A_1}{\partial x} - \frac{\beta_1}{2}A_1^2, \quad (1)$$

$$\frac{\partial A_2}{\partial z} = \mathrm{j}\sigma_2 A_1^2 \exp(-\mathrm{i}\Delta k z) - \frac{\alpha_2}{2}A_2 - \frac{\beta_2}{2}A_2^2, \quad (2)$$

where 1 and 2 denote the 556 and 278 nm waves, respectively, $\sigma_i = \omega_i d_{\mathrm{eff}}/n_i c$ is the second-order nonlinear coupling coefficient, n_i is the refractive index of CBO crystal, ω_i is the angular frequency, d_{eff} is the effective nonlinear coefficient of CBO crystal and $\Delta k = 2k_1 - k_2$ is the phase mismatch. ρ is the walk-off angle in the x-direction, α_i and β_i are the linear absorption and TPA coefficients, respectively. Here, $\rho = 11.6$ mrad, $\alpha_1 = 0.05\ \mathrm{cm}^{-1}$, $\alpha_2 = 0.07\ \mathrm{cm}^{-1}$, β_1 can be ignored and β_2 is assumed to be 6 cm/GW in our experimental condition.[21,22] In the case of our experiment, the Rayleigh range z_{R} of 556 nm beam with diameter of $w_0 = 90$ μm is calculated to be 70 mm by using

$$z_{\mathrm{R}} = \frac{\pi w_0^2 n_1}{\lambda_1}. \quad (3)$$

For crystal length < 70 mm, the input beam can be treated as a parallel beam and $\Delta k = 0$ for the ideal phase match. Equations (1) can be solved numerically by the fourth-order Runge–Kutte method. We calculated the UV average output power, pulse width and beam spatial distribution.

The calculated relationship of the output power with the pump power is also plotted in Fig. 2 with and without TPA by a black line and blue dashed line, respectively. As shown in Fig. 2, the calculated results with TPA are in close agreement with the experimental data. The slight deviation between the simulated values and the experimental data with the increasing pump power is most probably attributed to thermally induced phase mismatching (TIPM).[23] While the theoretical simulation without TPA overestimates the output power leading to 60%–80% higher at the full pump power. Therefore, we conclude that besides TIPM, TPA is a significant detrimental issue hindering high-power UV generation. Clearly, the theoretical model with TPA is more reasonable. In fact, TPA is inevitable when the total energy of two UV harmonic photons or one UV harmonic photon plus one visible photon reaches the cut-off wavelength, which lies around 170 nm for CBO crystal.[24] In general, TPA produces an increase of temperature in the crystal volume occupied by the beams and causes non-uniform temperature distribution in the bulk of crystal. Thermal gradient across the interacting beams in the crystal volume leads to thermal dephasing of the harmonic generation process, consequently resulting in the decrease of the FHG conversion efficiency. Concerning this issue, relevant improvement strategies would be in demand to alleviate this problem for scaling up the UV output power. Inspired by the research results in Refs. [25] and [26], we believe that keeping the operating temperature of the CBO at a high level would significantly mitigate the effect of TPA. Besides, a particular cooling mechanism for the CBO crystal may be also used to compensate the TIPM.[27]

The red dash-dot curve in Fig. 4 is the calculated pulse shape of the UV laser at the experimental condition. It is found that the measured and calculated pulse shape show a high level of similarity, but the simulated pulse duration (∼ 130 ns) is slightly less than that of measurement, which perhaps results from neglecting the TIPM in the theoretical calculation. Figure 5 shows the calculated 3D beam intensity distribution of 278 nm beam. The corresponding 2D intensity distribution is shown in the upper right corner of Fig. 5, indicating that the UV beam was elliptic with a circularity of ∼ 75%. Reasonably, the ellipticity of the laser mode mainly is attributed to the beam spatial walk-off in the x-direction for such a long CBO crystal.

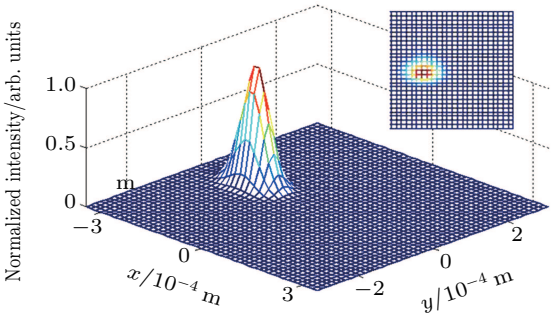


Fig. 5. Calculated 3D beam intensity distribution at 278 nm. Inset: calculated 2D beam profile.

4. Conclusion

We presented an efficient high power all-solid-state 278 nm UV laser based on FHG from a high-power nanosecond pulsed 1112 nm Nd:YAG MOPA laser in LBO and CBO crystals. Up to 10.3 W output power at 278 nm was obtained at the PRR of 2 kHz with the pulse duration of 140 ns, corresponding to the pulse peak power of 36.8 kW. To the best of our knowledge, this is the highest output level in terms of both average power and peak power for an all-solid-state UV laser between 275 and 300 nm. A theoretical model, which

takes into account of pump depletion, beam spatial walk-off, linear absorption and TPA in the Gaussian approximation of both spatial and temporal profiles, was employed to analysis the FHG process. The theoretical results with TPA were in close agreement with the experimental data and show that TPA in CBO crystal is a significant effect for UV generation, which leads to the thermal gradient in crystal and reducing the FHG efficiency. Aimed at this problem, relevant constructive strategies to alleviate the UV-induced degradation in CBO are proposed and higher UV output power can be expected.

Acknowledgment

We are grateful for the experimental assistance from Xiao-Wen Zhang and Ming Chen.

References

[1] Wang C, Wang G, Hicks A V, Dudley D R, Pang H and Hodgson N 2006 *Proc. SPIE* 6100
[2] Imai S, Matsuki K, Kikuiri N, Takayama K, Iwase O, Urata Y, Shinozaki T, Wada Y and Wada S 2010 *Proc. SPIE* 7580
[3] Tamhankar A and Patel R 2011 *J. Laser Appl.* **23** 032001
[4] Liu Q, Yan X, Fu X, Gong M and Wang D 2009 *Laser Phys. Lett.* **6** 203
[5] Bai Y, Li Y, Shen Z, Song D, Ren Z and Bai T 2009 *Laser Phys. Lett.* **6** 791
[6] Rajesh D, Yoshimura M, Eiro T, Mori Y, Sasaki T, Jayavel R, Kamimura T, Katsura T, Kojima T, Nishimae J and Yasui K 2008 *Opt. Mater.* **31** 461
[7] Xie S Y, Lu Y F, Zhang X F, Le X Y, Yang C L, Wang B S and Xu Z Y 2016 *Acta Phys. Sin.* **65** 184203 (in Chinese)
[8] Kojima T, Konno S, Fujikawa S, Yasui K, Yoshizawa K, Mori Y, Sasaki T, Tanaka M and Okada Y 2000 *Opt. Lett.* **25** 58
[9] Zhang N H, Fang S B, He P, Huang H D, Zhu J F, Tian W L, Wu H P, Pan S L, Teng H and Wei Z Y 2017 *Chin. Phys. B* **26** 064208
[10] Friedenauer A, Markert F, Kahra S, Schmitz H, Petersen L, Kahra S, Herrmann M, Udem TH Hansch T W and Schatz T 2006 *Appl. Phys. B* **84** 371
[11] Schmitt T, Puppe T A, Nendel A, Lison F, Kaenders W G and Flohic M L 2009 *Conference on Quantum Electronics and Laser Science* CLEO/QELS. Conference on IEEE 2009, p. 1
[12] Kaneda Y, Fallahi M, Hafer J, Moloney J, Koch S, Kunert B and Stoltzet W 2009 *Opt. Lett.* **34** 3511
[13] Wang Z C, Yang F, Zhang G C, Bo Y, Liu S S, Xie S Y, Xu Y T, Zong N, Li F Q, Liu B L, Xu J L, Peng Q J, Zhang J Y, Cui D F, Wu Y C and Xu Z Y 2012 *Opt. Lett.* **37** 2403
[14] Yang F, Liu B L, Wang Z C, Bo Y, Zhang G C, Peng Q J, Zhang J Y, Cui D F, Wu Y C and Xu Z Y 2014 *IEEE J. Quantum Electron.* **50** 423
[15] Singh S, Smith R G and Van Uitert L G 1974 *Phys. Rev. B* **10** 2566
[16] Liu B L, Wang Z C, Yang F, Wang Z M, Bo Y, Yuan H T, Yuan L, Wang B S, Xu J L, Guo Y D, Peng Q J, Zhang J Y, Cui D F and Xu Z Y 2014 *Chin. Opt. Lett.* **12** 45
[17] Liu B L, Wang Z C, Yang F, Wang Z M, Bo Y, Yuan H T, Yuan L, Wang B S, Xu J L, Guo Y D, Peng Q J, Zhang J Y, Cui D F and Xu Z Y 2014 *IEEE Photonics Technology Lett.* **26** 969
[18] Arisholm G 1997 *J. Opt. Soc. Am. B* **14** 2543
[19] Carrasco S, Saleh B E, Teich M C and Fourkas J T 2006 *J. Opt. Soc. Am. B* **23** 2134
[20] Sheng S C and Siegman A E 1980 *Phys. Rev. A* **21** 599
[21] Takahashi M, Osada A, Dergachev A, Moulton P F, Raduban M C, Shimizu T and Sarukura N 2010 *Jpn. J. Appl. Phys.* **49** 080211
[22] Divall M, Osvay K, Kurdi G, Divall E J, Klebniczki J, Bohus J and Peter A 2005 *Appl. Phys. B* **81** 1123
[23] Sabaeian M, Jalil-Abadi F S, Rezaee M M and Motazedian A 2014 *Opt. Express* **22** 25615
[24] Wu S, Blake G A, Sun S and Yu H 2000 *Proc. SPIE-The International Society for Optical Engineering* 3928
[25] Takachiho K, Yoshimura M, Takahashi Y, Imade M, Sasaki T and Mori Y 2014 *Opt. Mater. Express* **4** 559
[26] Yap Y K, Inoue T, Sakai H, Kagebayashi Y, Mori Y and Sasaki T 1998 *Opt. Lett.* **23** 34
[27] Yap Y K, Deki K, Kitatochi N, Mori Y and Sasakiet T 1998 *Opt. Lett.* **23** 1016